Newcastle University

ePrints

Duan F, Hu Z, Niedzwecki J. Model test investigation of a spar floating wind turbine. *Marine Structures* 2016, 49(2016), 76-96.

Copyright:

© 2016. This manuscript version is made available under the CC-BY-NC-ND 4.0 license

DOI link to article:

http://dx.doi.org/10.1016/j.marstruc.2016.05.011

Date deposited:

11/10/2016

Embargo release date:

06 June 2017

This work is licensed under a
Creative Commons Attribution-NonCommercial-NoDerivatives 4.0 International licence

Newcastle University ePrints - eprint.ncl.ac.uk

Model Test Investigation of a Spar Floating Wind Turbine

Fei Duan[a,b], Zhiqiang Hu[a,b,*], and J. M. Niedzwecki[c]

a. State Key Laboratory of Ocean Engineering, Shanghai Jiao Tong University, Shanghai, China

b. Collaborative Innovation Center for Advanced Ship and Deep-Sea Exploration, Shanghai Jiao Tong University, Shanghai, China

c. Zachry Department of Civil Engineering, Texas A&M University, College Station, Texas, 77843-3136, USA

Abstract

Several floating wind turbine designs whose hull designs reflect those used in offshore petroleum industry have emerged as leading candidates for the future development of offshore wind farms. This article presents the research findings from a model basin test program that investigated the dynamic response of a 1:50 scale model OC3 spar floating wind turbine concept designed for a water depth of 200 m. In this study the rotor was allowed to rotate freely with the wind speed and this approach eliminated some of the undesirable effects of controlling wind turbine rotational speed that were observed in earlier studies. The quality of the wind field developed by an array of fans was investigated as to its uniformity and turbulence intensity. Additional calibration tests were performed to characterize various components that included establishing the baseline wind turbine tower frequencies, stiffness of the delta type mooring system and free decay response behavior. The assembled system was then studied under a sequence of wind and irregular wave scenarios to reveal the nature of the coupled response behavior. The wind loads were found to have an obvious influence on the surge, heave and pitch behavior of the spar wind turbine system. It was observed from the experimental measurements that bending moment at the top of the support tower is dominated by the 1P oscillation component and somewhat influenced by the incoming wave. Further it was determined that the axial rotor thrust and tower-top shear force have similar dynamic characteristics both dominated by tower's first mode of vibration under wind-only condition while dominated by the incident wave field when experiencing wind-wave loading. The tensions measured in the mooring lines resulting from either wave or wind-wave excitations were influenced by the surge/pitch and heave couplings and the wind loads were found to have a clear influence on the dynamic responses of the mooring system.

Key words: offshore wind turbine; spar-hull; physical model test; aero-hydro coupling effects

* Corresponding Author. State Key Laboratory of Ocean Engineering, Shanghai Jiao Tong University, 800 Dongchuan Road, 200240, China.

E-mail address: zhqhu@sjtu.edu.cn (Zhiqiang Hu)

1. Introduction

With the continually increasing worldwide demand for energy coupled with a growing public awareness of the need to protect the environment, clean renewable energy has become an important current research and development. The conversion of energy from the wind and solar sources are the most visible in terms of research and application to commercial enterprises. Because traditional fixed seafloor-mounted offshore wind turbines are prohibitively expensive in deep water (Sclavounos, Tracy and Lee, 2008), industry and researchers have gradually begun to focus on a variety of floating offshore wind turbines concepts. This research study deals with a deepwater spar-type offshore wind turbine concept that could be deployed beyond the line of sight of populous coastal regions and yet near enough to population centers that could benefit energy generating from steadier and stronger wind resources. The research with respect to floating offshore wind turbines is multidisciplinary, involving aerodynamics, hydrodynamics, multi-structure dynamics (elastic) and automatic control (Namik and Stol, 2010; Wang and Sweetman, 2013; Jeon and Lee, 2014; Salehyar and Zhu, 2015; Nejad et al., 2015). So that it is of great importance to reveal the nature of dynamic response characteristics for the in-depth analysis and accurate assessment with respect to a spar-type floating offshore wind turbine (FOWT).

In recent years, the study and analysis of floating wind turbines has mainly relied on simulation tools capable of predicting the coupled dynamic loads and responses of the floating system. In Phase IV of the Offshore Code Comparison Collaboration (OC3), it proposed a floating wind turbine using the specifications of the NREL 5-MW Baseline Wind Turbine (Jonkman et al., 2009), except the properties of support structure (tower and substructure) and control system (Jonkman, 2010). The modified floater used to support the NREL 5-MW Baseline Turbine is called OC3-Hywind in (Jonkman, 2010), and the modified tower is called the "OC3 Hywind tower" in this paper. Soon afterwards, the Code Comparison Collaboration Continuation (OC4) Project was launched by the IEA as an extension of OC3. Both the OC3 and OC4 projects sought to verify the accuracy of the offshore wind turbine dynamics simulation tools (or codes) through a code-to-code comparison of simulated responses of various offshore structures (Jonkman et al., 2012; Robertson, Jonkman and Musial, 2013). Many simulation tools have been developed and improved for the fully coupled analysis of floating wind turbines (Karimirad, M., 2011; Kvittema, Bachynski, and Moan, 2012; Quallen, et al., 2013; Bae, Kim and Shin, 2010; Gueydon and Xu, 2011) and many of these simulation tools have been compared and analysed in the OC3 and OC4 projects. However, due to the complexity of these models, the accuracy and reliability of these predictive tools still requires more validation with measured data from real floating offshore wind turbines or model tests.

Statoil and Principle Power Company have conducted field data collection for Hywind and WindFloat respectively, but their recorded field data have not been released for use to the general research community. Thus, model basin test programs focused on floating wind turbines are essential to verify the simulation tools being conceived and developed by researchers around the world. In 2006, Nielsen, Hanson, and Skaare, reported on a model 1:47 scale model test of a 5-MW spar floating wind turbine conducted at Marintek for the Hydro Oil & Energy Company (Neilson, et al., 2006). It presented control schemes based on below or above rated wind speed condition for a basin model in line with those applied on real FOWT. The Principle Power Corporation performed a 1:67 scale model test in the development phase of the first full scale WindFloat platform (Cermelli, et al., 2010). Due to the unmatched Re number effect so that the lower model axial rotor thrust and the exceeding complication of control applications in model testing, a compromise was adopted by using a circular disc rather than turbine blades to obtain the equivalent thrust force. This scheme focused on the thrust force (one of the most important aerodynamic loads) and neglected other aerodynamic loads of turbine, providing an alternative solution to eliminate the undesired effect of unmatched Re number. In 2011, Shin (2011) conducted a model test with a 1/128 scale ratio in Ocean Engineering Wide Tank at University of Ulsan. This work modelled the OC3-Hywind floating wind turbine and utilized model blades in

place of drag disc, which can offer a reference for follow-up experiment and simulation researches with respect to OC3 FOWT. The WindSea Company conducted a model experiment for their WindSea spar-hull wind turbine concept at a 1:64,29 Froude scale (WindSea, 2012). It proposed a new FOWT concept and aimed at verifying their theoretical model. More recently, the University of Maine conducted a series of 1:50 scale model tests incorporating spar-type, semi-submersible-type and TLP-type floating wind turbine concepts (Martin, et al., 2012; Koo, et al., 2012; Goupee, et al., 2012). These works described the test methodology, model specifications, instrumentation set-up and external environment definition in detail. Also reported in these publications are the primary results of the model basin tests. As a further stage of the basin experiment, a 1:50 scaled model test with respect to the GustoMSC Tri-Floater concept was performed at MARIN basin (Huijs, de Ridder and Savenije, 2014). This work presented a new model rotor blade with a better Ct and Cp performance under Froude-scaled wind speed, and their control applications were also reported. Furthermore, a STC (spar Tours Combination) concept model test was conducted by Norwegian University of Science and Technology (NTNU) in the towing tank of MARINTEK with a 1:50 model scale (Wan, Gao and Moan, 2014). A new combination concept of FOWT and WEC was proposed in this work, and the reliability of this combination concept in survival modes was also investigated. These aforementioned study approaches which involve computer simulation, prototype data measurement and model tests are summarized in Table 1.

Table 1. Summary of selected studies on floating wind turbines

Author/Organization	Year	Classification	Approach	Model Type	Scale Ratio	Contributions	Comments
Jonkman, et al. (2009)	2009	OC3	code-to-code comparison	-	-	established a baseline wind turbine concept	opportunity for comparison with prototype floating wind turbine data or model data
Jonkman (2010)	2010		code-to-code comparison	-	-	proposed a spar-type floating wind turbine concept	
Jonkman, et al. (2012)	2012	OC4	code-to-code comparison	-	-	simulation of a jacket-supported FOWT	
Robertson, et al. (2013)	2013		code-to-code comparison	-	-	simulation of a semi-type FOWT	
Statoil & Principle Power	-	prototype measurement	data collection from Hywind and WindFloat	-	-	validation for simulation tools	proprietary data
Hydro Oil & Energy (Nielsen, et al., 2006)	2006	model test	-	5 MW Hywind	1:47	proposal of control scheme for model testing	some details not available
Principle Power (Cermelli et al., 2010)	2010		-	WindFloat model	1:67	an alternative solution for	validation of hydrodynamic

						remedying unmatched Re number effect	portion of simulation tools
University of Ulsan (Shin, 2011)	2011		-	OC3-Hywind FOWT	1:128	convenient for follow-up researches with respect to this concept & model blades rather than drag disc	limited result publication
WindSea Company (WindSea website)	2012		-	WindSea model	1:64,29	proposal of a new FOWT concept	aimed at verifying their theoretical model
University of Maine (Martin et al., 2012; Koo, et al., 2012; Goupee, et al., 2012)	2012		-	spar, Semi-submersible and TLP	1:50	detailed description of test set-up, model specifications and experiment methodology	some details not available
GustoMSC	2014		-	three-column semi-submersible	1:50	proposal of new model blades with a better Ct and Cp performance & control scheme application	not fully representative for the full scale control system & rotor thrust force not fully simulated under Froude-scaled wind speed
NTNU	2014		-	STC	1:50	an innovative renewable offshore concept	wind disc instead of blade-rotor system & cannot validate traditional simulation tools

Although some model tests have been conducted by MARIN and other research institutions, paper publications in public domain involving these basin test results are still relatively limited, which cannot keep pace with the current developing levels of corresponding simulation tools. More woks should be performed in an effort to satisfy the urgent validation need of existing floating offshore wind turbine (FOWT) simulation codes. In addition, as the research institution whose model test procedures regarding FOWT have the largest number and the most comprehensiveness, MARIN mainly published the test results based on semi-submersible floaters (Martin, et al., 2012; Gueydon and Weller, 2012; Coulling, et al., 2013; Koo, et al., 2014; Huijs, de Ridder and Savenije, 2014; Allen, et al., 2015; Huijs, 2015), publications of test results with respect to the spar-type supported FOWT are relatively rare, resulting in an inability to provide

comprehensive enough validation data. Further, emphasises of these published papers were placed on describing test techniques, presenting raw test data or on comparisons between measured and simulation results to validate simulation tools. In-depth analysis of dynamic response characteristics and coupled behaviours of a spar-type FOWT was rarely conducted.

The intent of this research study was to provide new model test data regarding a spar-type FOWT that will complement that presently available to researchers and overcome the deficiency in shortage of test result publications of FOWT based on a spar-type floater. In addition, more important focus of this paper is on conducting in-depth analysis of response behaviour characteristics of the spar-type wind turbine and corresponding conclusions are subsequently presented. Particular attention is directed at the details that include of the spar model and rotor design, the mooring system, the careful characterization of the wind field, and the anticipated coupling of the response behaviour. Although this basin test is referred to that conducted by MARIN, unique approaches have been implemented in this test such as the rotor spinning was completely induced by the applied wind loads rather than motor-drive, which is closer to the real wind turbine operation scheme, and the increasing level of model wind speed was relatively reduced, resulting in less undesired additional drag on the non-rotor components. The results of this model test can also provide a contrast with those of MARIN to prove the reliability of their results. The experiment technologies, results and conclusions in this document should be a good validation tool for current simulation codes and a good technology accumulation and reference for future developments in the field of FOWT model testing.

2. Floating wind turbine model experiment particulars

2.1 Spar model

A picture of the 1:50 Froude-scaled model spar wind turbine developed for this experimental research investigation is presented in Figure 1.

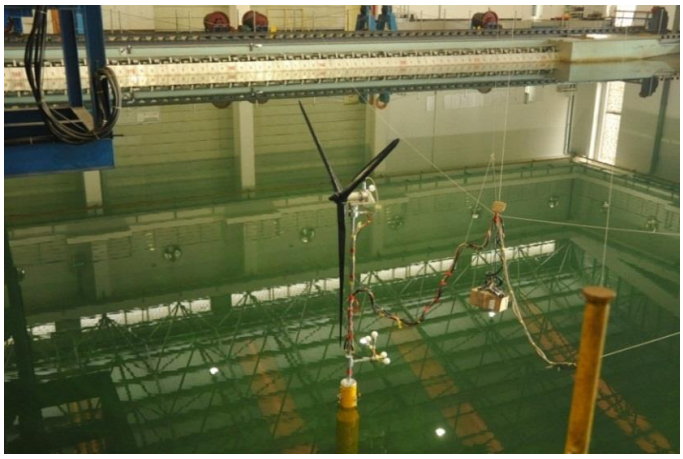

Figure 1. spar-type floating wind turbine model in the SJTU deepwater model basin

The design of the spar-type hull model was based on the OC3 Hywind floater (Jonkman, 2010) and is illustrated in Figure 2. In Table 2 the information is presented at prototype scales (Robertson, et al., 2013), and the still water level is abbreviated as SWL and the negative sign indicates an elevation below the SWL. It should be noted that all the center of mass (CM) locations are with respect to the SWL in this paper unless specified. It was observed that the wind turbine was overweight, and the center of mass (CM) location was slightly lower than the target value (this will be stated in detail below). To compensate for these effects on the mass and CM of the entire floating system, it was decided to that the model should attempt to closely replicate the prototype total floating system mass and to approach its CM value as closely as possible.

Implementing this rule, the hull parameters are listed in Table 2. The results of this approach are reported in Table 3 and the agreement is quite good (Koo, et al., 2012). It can also be observed in Table 2 that the roll and pitch moments of inertia for the spar hull are somewhat larger than the target values. As demonstrated in Table 3, the full-scale mass of the entire model floating system in this experimental study is very close to that of the targeted with less than 1% error and the CM error of the entire floating system is also on the same order of magnitude.

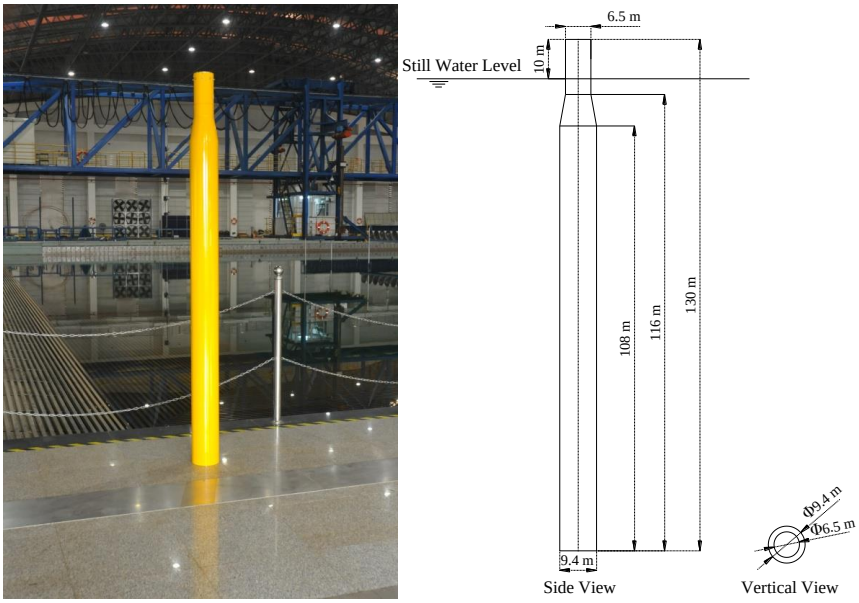

Figure 2. Photograph and Main Dimensions of spar-type Floater

Table 2. Main properties of the spar-type hull

Item	Unit	NREL	Measurement for SJTU's Test	Measurement for MARIN's Test
Platform Mass, including Ballast	kg	7,466,330	7,316,578	7,281,600
CM Location below SWL along the Platform Centreline	m	-89.9155	-94.1495	-91.1
Platform Roll Inertia about the CM	kg•m^2	4,229,230,000	4,656,382,813	3,966,000,000
Platform Pitch Inertia about the CM	kg•m^2	4,229,230,000	4,656,382,813	3,966,000,000
Platform Yaw Inertia about the Platform Centreline	kg•m^2	164,230,000	not measured	98,600,000

Table 3. Comparison of the mass and CM of the entire floating system

NREL		Measurement for SJTU's Test		Measurement for MARIN's Test	
Mass (kg)	Centre of mass (m)	Mass (kg)	Centre of mass (m)	Mass (kg)	Centre of mass (m)
8,066,048	-78	8,066,109	-78.947	7,980,000	-76.35

2.2 Wind turbine and blade models

The wind turbine model was designed and fabricated to emulate the prototype parameters in NREL's 5-MW wind turbine for the OC3 project (Jonkman, et al., 2009; Jonkman, 2010). The blade model properties reported by Martin (2011) were utilized to fabricate the blade models. Particular care was taken in the

material selection and the manufacturing process to simultaneously achieve the target length of 1.23 m and a mass of only 138.46 g. The model blade was fabricated as a hollow structure with two thin layers of woven carbon fibre epoxy composite material join together. The interior of the hollow blade model was filled with a carbon fibre stick wrapped in resin. The total length of the combined filling material was less than half the length of the blade model, and additionally the resin was perforated to reduce the mass. The total blade model mass was measured to be 137 g, which is 1.05% lighter than that required. An image of a model blade used in this study is shown in Figure 3.

Figure 3. Image of a fabricated composite blade

The design and fabrication of the tower was also based on the tower properties in the model test program of University of Maine as reported by Martin (2011). However, there were three differences that are important to recognize. First, the bottom of the tower was designed for a perfect connection onto the hull. In the report by Martin (2011), an aluminium 2024 alloy was selected for the bottom section between the shaft collar and bottom of the tower, due to its high strength to withstand a significant bending moment during model testing. In this study, an aluminium 6061 alloy was selected, as it provides nearly the same stiffness and strength but a higher resistance to deterioration in the humid model basin environment. The third difference was that the top section of the tower was adjusted to match the load cells # 1 as shown in Figure 4. An aluminium connector was originally designed to provide a connection between the nacelle and the tower. The load cells # 1 was located below this part to capture the 6 DOF forces and moments between the nacelle and tower. Consequently, the length of middle section of the tower was 1437.78 mm rather than the 1222.38 mm reported by Martin (2011). A photograph and schematic of the tower design is presented in Figure 4. For convenience, the dimensions of the tower are presented in model scale. The total mass of the tower model was determined to be 2.241 kg with a CM located at 0.82m above the tower base. The masses and CM locations of the main components used in the wind turbine are listed at prototype scale in Table 4 (Jonkman et al., 2009; Jonkman, 2010). Martin (2011) reported the mass and CM of tower without instrumentation cables, and Coulling et al. (2013) presented the mass and CM of tower with instrumentation cables. So the parameters of instrumentation cables can be calculated from these two publications. In addition, as mentioned by Coulling et al. (2013), the hub height is 90 m and the shaft tilt and precone is null so that the CMs of hub and three-blade of MARIN's test in the vertical direction can be speculated both at 90 m above SWL. Further, based on Table 4, the nacelle CM of MARIN's test can be calculated as 92.29 m. There was a bundle of instrumentation cables that run along most of the tower for the physically tested model, and as shown in Table 4, the effect of instrumentation on the turbine mass and CM are mainly contributed by the sensor cables for both our and MARIN's test.

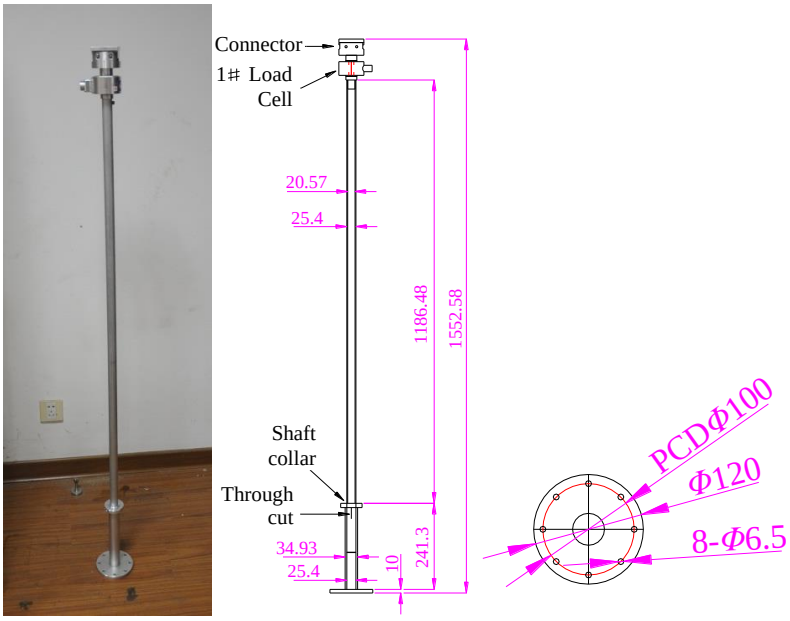

Figure 4. Photograph and schematic diagram of wind turbine support tower

Table 4. Mass and CM location of main components of wind turbine

	NREL		Measurement for SJTU's Test		Measurement for MARIN's Test	
Item	**Mass (kg)**	**Centre of mass (m)**	**Mass (kg)**	**Centre of mass (m)**	**Mass (kg)**	**Centre of mass (m)**
Blade (three in total)	53,220	90	52,659	90.65	48,750	90
Hub	56,780	90.17	57,272	90.65	72,880	90
Nacelle	240,000	89.35	232,291	90.65	274,900	92.29
Tower	249,718	43.4	287,128	51	164,600	44.45
4 markers at tower bottom	-	-	27,163	30.9	-	-
1 marker at nacelle	-	-	6,791	92.15	-	-
Instrumentation cables	-	-	86,228	57.1	137,640	44.78
Total Wind turbine	599,718	70.35	749,531	69.45	699,400	71.2

The shaft tilt of 5° was not accounted for in the model construction, which was also the case for MARIN model test program (Martin, 2011). Besides, only the vertical CM along the tower centreline was considered in Table 4. The total CM location of the wind turbine atop the tower was adjusted onto the tower centreline. A photograph showing the assembly model wind turbine attached to a foundation base is presented in Figure 5.

Figure 5. Assembled wind turbine model

2.3 Mooring system design

The prototype water depth modelled in the experiment was 200 m and was consistent with MARIN's tests (Koo, et al., 2012). For the model basin experiments conducted at MARIN, Koo, et al. (2012) reported that their taut mooring system utilized a delta connection to simulate the Statoil Hywind configuration. The layout of the mooring system configuration is presented in Figure 6. The bold circle represents spar hull, the other lines illustrate the location of the mooring lines with fairleads located at the intersection of two mooring lines originating from the hull (Duan, Hu and Wang, 2015). Also noted are the three tension sensors that were used to measure the tension of the mooring system. The-full-scale properties of the mooring system are listed in Table 5 and are based on those reported by Koo, et al. (2012).

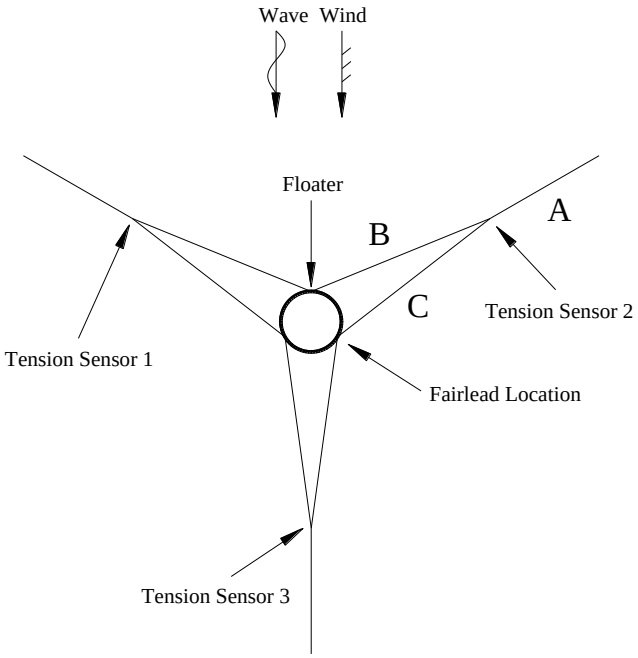

Figure 6. spar hull and mooring system layout

Table 5. Principal properties of the taut prototype mooring system

Item	Unit	Designations
Number of mooring lines	-	3 for type A; 6 for type B or C
Angle between two mooring lines of type A	deg	120
Anchor Radius	m	445
Anchor Depth	m	200
Radius of Fairlead	m	5.2
Fairlead Depth	m	70
Unstretched Line Length A	m	424.35
Unstretched Line Length B & C	m	30
Line A Diameter	m	0.167
Line B & C Diameter	m	0.125
Mass per Length Line A (dry)	Kg/m	22.5
Mass per Length Line B & C (dry)	Kg/m	12.6
Axial Stiffness Line A (EA)	N	121,000,000
Axial Stiffness Line B & C (EA)	N	68,000,000

2.4 Wind system design

To accurately capture the coupled behaviour under simultaneous aerodynamic and hydrodynamic loading, it was important to design and build a wind generation system capable of providing a controllable wind field. The system developed for this research study is pictured in Figure 7. It consisted of 9 independently controllable axial fans in a 3 x 3 stacked square configuration. The dimensions of the effective wind output area are 3.76 m times 3.76 m. The system can be used to generate model wind speeds up to 9.53 m/s. To enhance the wind environment quality for steady wind speeds, a honeycomb screen was attached to the front of the wind generation system.

Figure 7. SJTU Wind Generation System

2.5 Model instrumentation

To accurately capture the dynamic loads and accelerations experienced by this moored spar-type floating wind turbine system, a series of instruments were configured as shown in Figure 8. The origin, R, of this reference coordinate system is taken at the intersection of the tower centreline and the still water plane surface, where RX pointed to the north (opposite direction of the wind and waves) and RY pointed to the

west. The 6 DOF forces and moments for the two load cells, as well as 3 DOF accelerations, are also shown in the schematic. Note that the direction of the wind and wave loads always pointed in 180 °orientations with respect to the floating wind turbine during all the model basin tests and that Acex, Acey and Acez refer to accelerations in the x, y and z directions, respectively.

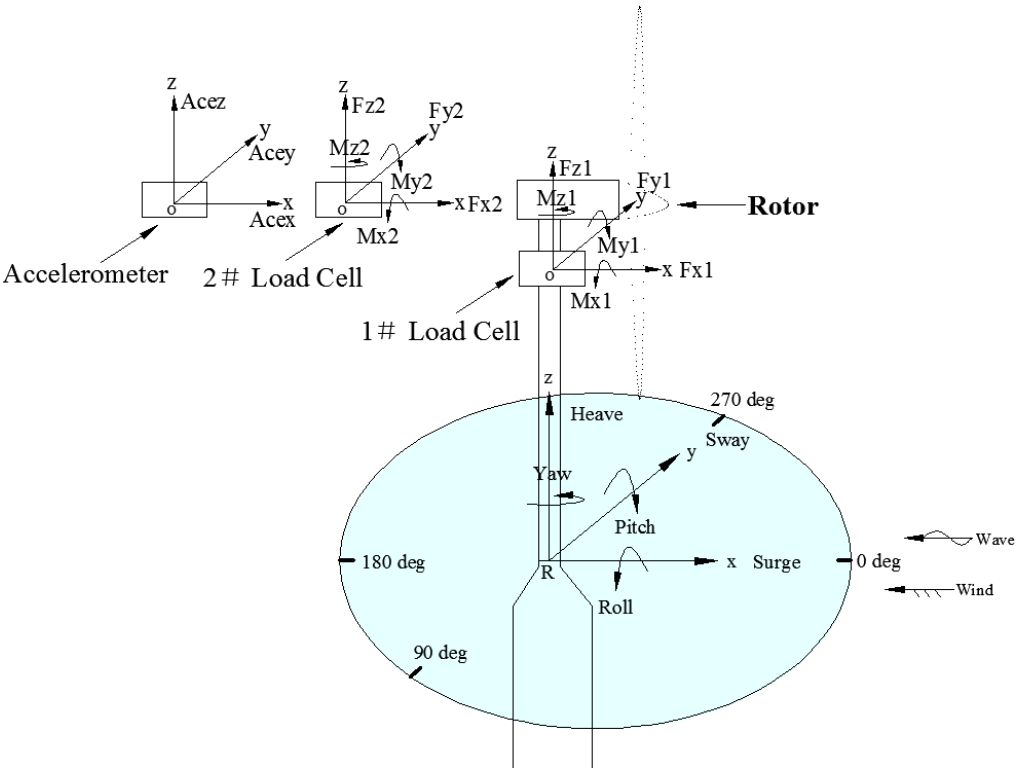

Figure 8. Definition of coordinates for 6 DOF motions, forces, moments and accelerations

Load cell # 1 was located between the nacelle and tower to measure the 6 DOF forces and moments between them, and load cell # 2 was located in the nacelle to capture the 6 DOF forces and moments in the nacelle. An accelerometer was installed in the rear of the nacelle to measure the 3 DOF nacelle accelerations. In this experiment, an active optical motion capture system was utilized to measure the six DOF motions of the floating system and four active optical markers fixed at the end of the tower. Several of these important aspects are noted in the photographs presented in Figure 9. Additionally, three tension sensors were located at the joints of the two short mooring lines (B and C line) to measure the tension of the mooring lines, as shown in Figure 6.

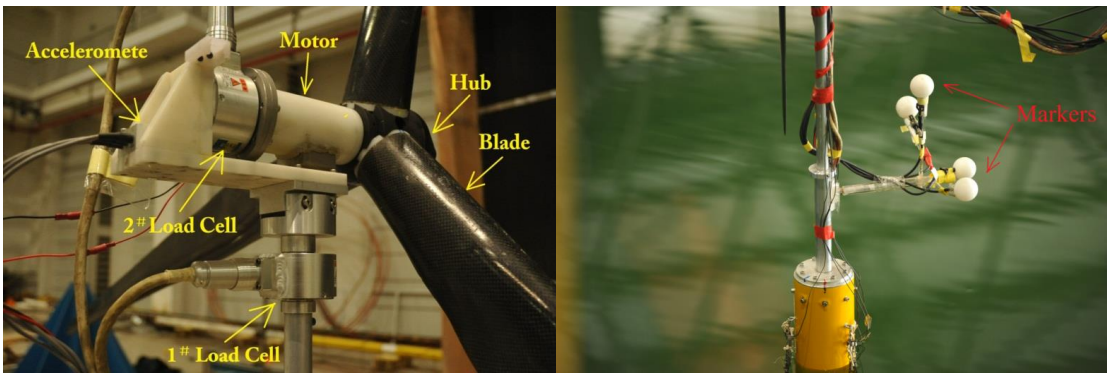

Figure 9. Accelerometer, load cell and optical markers mounted on floating wind turbine

3. Preliminary calibration experiments

Prior to the basin tests, a series of calibration tests were conducted. The quality of the wind field was investigated to determine the spatial homogeneity and turbulence intensity of the wind field that would be utilized in the test program. Next the wind turbine tower configuration was fixed to the model basin perimeter and subject to the range of planned wind conditions in order to calibrate the relationships between the wind speed, rotor thrust, rotor speed and frequency of the wind-making machine drive. A hammer test of the tower was also utilized to evaluate the natural frequencies of the tower. In the model basin the system behaviour of the moored spar hull configuration was investigated to verify the restoring stiffness of the mooring system and a free decay test was also conducted to identify the natural periods of the integrated floating wind turbine system. Additional details of these calibrations are reported in this section.

3.1 Investigation of the Wind field

The quality of the wind to be generated during the model test program was investigated using an array of DANTEC Dynamics MiniCTA anemometers with a 20 Hz sampling frequency. The array was designed to measure the time-series of the wind at forty-five measurement points and is illustrated in Figure 10. As shown the array consisted of nine measurement points along the horizontal direction arranged at five different vertical elevations. This array was positioned 3 m downstream from the wind generation system based upon the typical distance between the floating wind turbine system and the wind generating system during the model basin testing. The objective was to characterize the spatial wind speed uniformity and the turbulence intensity in the near field of the spar-type floating wind turbine model.

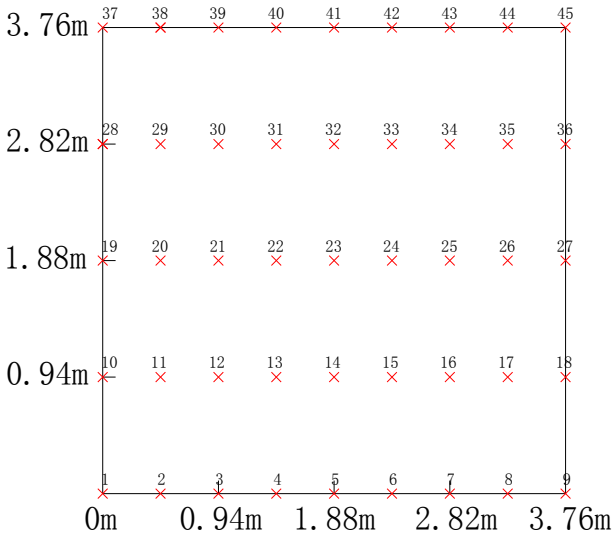

Figure 10. Location of the wind field measurement points in the array

Examples of the approach used in the characterization of the wind field are presented in Figures 11, 12 and 13. The uniformity of the wind speed and the turbulence intensity are presented in Figure 11 at model scale based on a targeted wind-making machine frequency of 6.2 Hz which represents the 5 m/s wind velocity load case, as listed in Table 6. The wind speed surface as shown represents the smoothed mean wind velocity values of the time histories, and the turbulence intensity surface is the corresponding temporal standard deviation of the time histories divided by the mean wind speed of the time history at each point in the grid (Fowler et al., 2013). The solid black circle is used to define the rotor plane in the wind field, and the black cross at its center indicates the positioning of the hub center at the x=1.88 m, y=1.506 m.

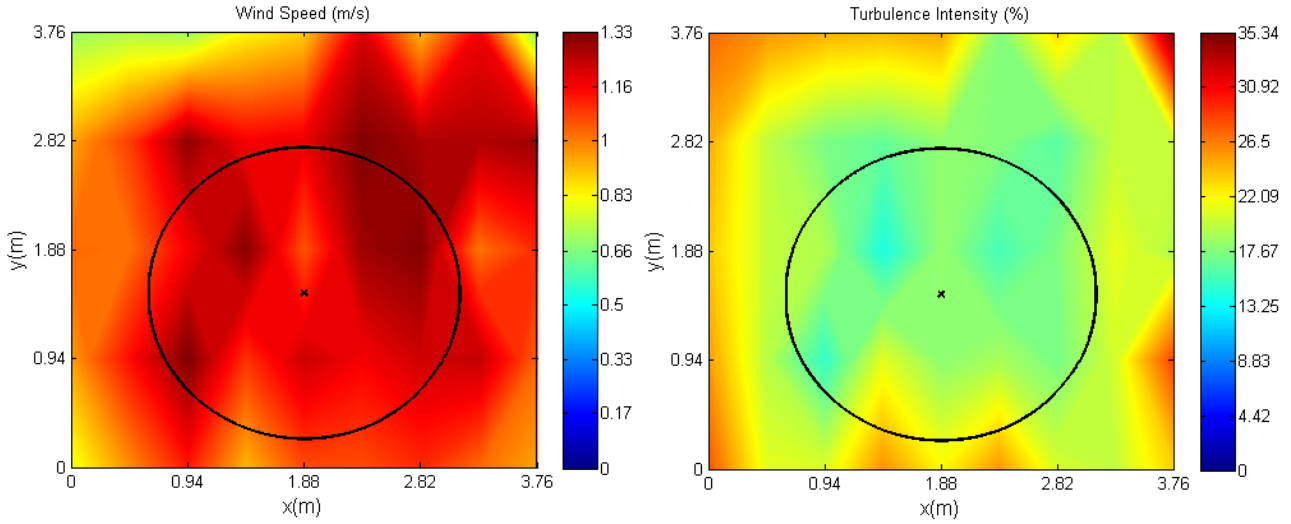

Figure 11. Wind Speed Profile and Turbulence Intensity at the spar wind turbine model location

As observed from these two figures, the spatial uniformity of the wind field is fair, and the turbulence intensity is generally lower than 20% within the rotor plane. To further illustrate the variability of the wind field, a sample time history of the model wind speed at the 23rd measurement point is plotted in Figure 12. This point was chosen because in the array it is the location closest to the hub center.

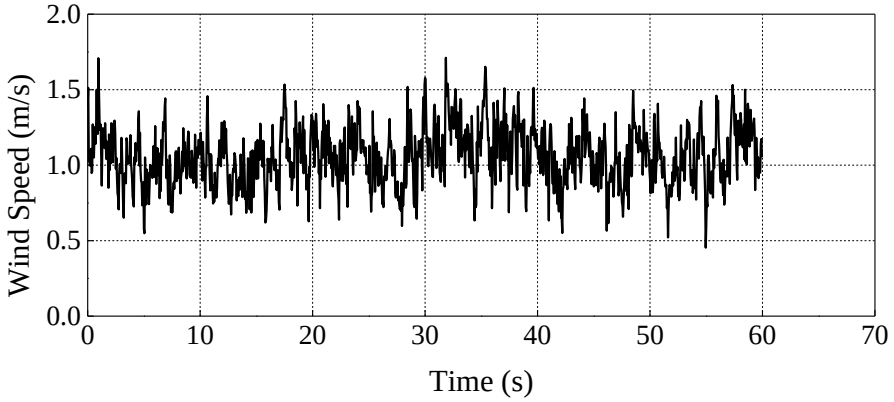

Figure 12. Sample time history of the wind speed at measurement point number 23

Two additional points in the array were selected for comparison, the 22nd and 32nd, due to their close proximity to the 23rd point. Figure 13 presents the power spectral densities (PSDs) at model scale with respect to the wind speed based on the time histories recorded at the three sensor locations. The curves of computed spectra in Figure 13 all show similar monotonically decreasing characteristics at low angular frequency because there exists a fluctuation with a long period and high amplitude in the time history for these three points, which also can be seen in Figure 12. This characteristic results from the unsteadiness of the wind generation system and will have an influence on the motions and loads related to the wind loads. Taking surge or pitch response behaviour as an example, the PSD of the surge or pitch based on the wind-only load condition will also have a monotonically decreasing curve in the low frequency zone because of the low-frequency change property of the wind field. Additionally, there exist spectral peaks at high angular frequencies in the results of the PSDs for these points, such as 4.29 rad/s for the 23rd or 3.77 rad/s for the 32nd.

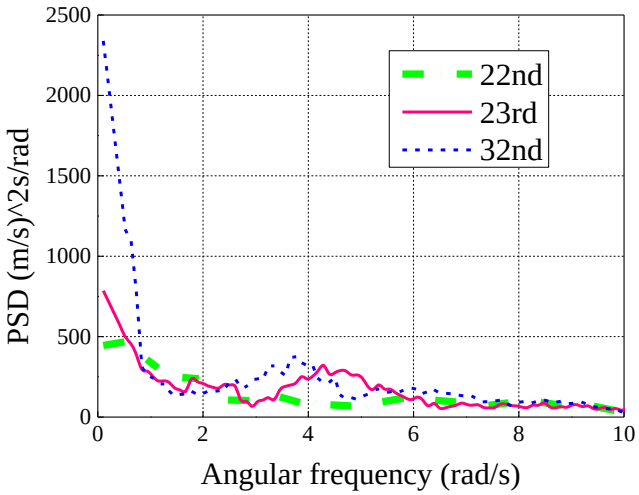

Figure 13. Spectral density of the measured wind speed at model scale at three measurement points

3.2 Wind turbine free blade rotation approach

Prior to basin testing, the fixed wind turbine test was performed. In this experimental study a different approach was taken that allows the rotor to turn freely to the incident wind field. During these measurements, the wind turbine was mounted on a fixed based on land in front of the wind generator system. The distance from the wind generator and the relative hub height kept the same as the parameters of basin configuration. The purpose of the fixed base wind turbine test was to obtain the target rotor thrust by adjusting the frequency of the wind-making machine drive and consequently increasing the wind speed. In this test, to better simulate the prototype rotor operational state, the rotor motion was completely induced by the applied wind loads. Pitch control of the wind turbine blades was not considered in this test program. Because the Froude scaling is implemented in this model test, the Reynolds number for the model basin experiments will be lower and consequently the model rotor thrust and torque will also both be lower than the target values scaled from the prototype. Therefore, to achieve the proper thrust force under each wind speed condition, the wind speed has to be increased, and the rotor rotational speed will vary accordingly. For example, under the 5 m/s prototype wind speed condition, the prototype rotor thrust is 276 kN. Therefore, the frequency of the wind-making machine drive was adjusted until the rotor achieves the target prototype rotor thrust. The wind speed at the hub centre location with respect to this desired frequency, 6.2 Hz was then measured. When performing basin testing, the frequency of the wind-making machine drive was adjusted to 6.2 Hz to simulate this 5 m/s prototype wind speed condition. The relationships between the wind speed, rotor thrust, rotor speed and frequency of the wind-making machine drive for the prototype and measurement were determined and listed in Table 6. Note that the prototype parameter values are also presented in Table 6 for comparison and that the wind speeds are based on the data measured at the wind turbine hub height (Koo, et al., 2012).

Table 6. Fixed Wind Turbine Test Results

Prototype	Wind Speed (m/s)	5	8	11.4	18	23	40
	Rotor Speed (rpm)	7.5	9.3	12.1	12.1	12.1	0
	Rotor Thrust (kN)	276	494.9	770.4	451.1	388.9	145
Measurement	Wind Speed (m/s)	9.4	11.4	12.8	11.1	10.9	15.7
	Rotor Speed (rpm)	7.9	11.2	14.4	10.9	10.6	0
	Rotor Thrust (kN)	276	494.9	770.4	451.1	388.9	145
	Frequency of Wind-Making	6.2	7.4	8.3	7.3	7.2	10

	Machine Drive (Hz)						

It should be noted that the rotation of the model rotor was suspended for the 145 kN rotor thrust case as the prototype rotor is parked in this extreme 40 m/s wind condition. The measured wind speed decreases when the prototype wind speed is higher than the rated wind speed because no blade-pitch was performed during this test so that the model wind speed was intentionally reduced with the purpose to obtain the desired rotor thrust.

The differences, advantages and disadvantages to modelling approach taken in this research study compared to MARIN's test program are highlighted in Table 7.

Table 7. Difference from MARIN physical model tests

Difference	Item	MARIN	SJTU
advantage	rotor rotation actuator	motor-drive	wind-drive
	increasing degree of wind speed	high	low
disadvantage	matching degree of the rotor speed with the desired values	high	relatively low

In the experiments conducted at the MARIN Basin, a motor installed in the wind turbine nacelle controlled the rotor rotation. The rotor rpm was set to a required value for each case (Koo, et al., 2012). This approach means that the rotation of the rotor was induced by the motor-drive and not by the wind loads and consequently resulted in a rotor speed relatively close to the target value. However, a drastic increase in the wind speed was required to achieve the desired thrust. For example, for the rated prototype wind speed case with an 870-kN rotor thrust based on spar floater offshore (Goupee, et al., 2012) (equivalent to 770.4-kN rotor thrust based on fixed wind turbine onshore in this test presented in Table 6), the wind speed was increased from 11.4 m/s to 20.8 m/s to match the required thrust and this actually produced the undesirable excess drag on non-rotor structures (Martin, 2011). In contrast, for this study the rotor rotation was completely induced by the wind loads, which is more closed to the real wind turbine operational situation, and substantially reduced this undesirable excess drag effect. For example taking for this case the wind speed only required an increase in wind speed to 12.8 m/s, compared to the 20.8 m/s. By applying this technique, the undesired effects induced by the increase in the wind speed were minimized. To evaluate the variation of the measured rotor speed compared to the target value due to free spinning, the normalized rotor speed based on the values presented in Table 6 are plotted in Figure 14.

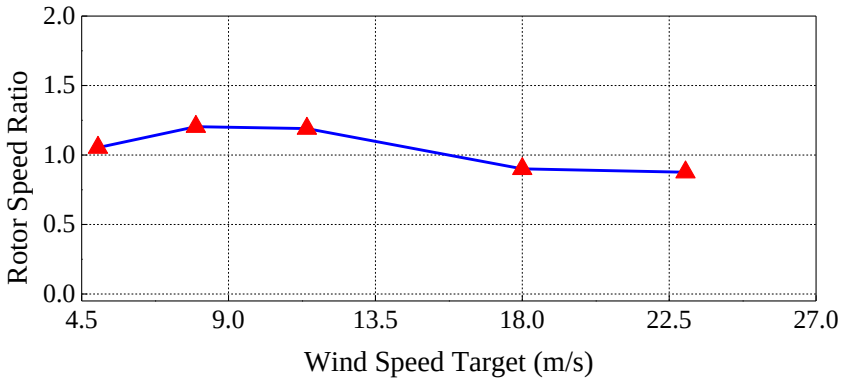

Figure 14. Normalized rotor speed and targeted wind speed for free rotor system used in this study.

These five rotor speed ratio points (based on the first five wind speed in Table 6) marked by red triangles should have a value of unity with increasing prototype wind speed. The nearness of the ratio to unity suggests that the variation of the measured rotor speeds presented in Table 6 is quite reasonable and that the use of freely turning rotors is an acceptable approach.

3.3 Frequency response of the wind tower

The natural structural frequency of the wind turbine tower was evaluated using a hammer test procedure. The rotor and nacelle were not included in this test configuration. For the test, the tower was rigidly connected to the land via a load cell that can measure the bending moment caused by the tower vibration. The impulse excitation was applied to the tower top, causing it to vibrate freely. The time history of the vibration-induced bending moment was then recorded, and the power spectral density of the response evaluated. The multi-peaked response spectrum is presented in Figure 15. As seen there are two dominant peaks, the smaller one at 2.6 rad/s and the much larger one excited at 4.21 rad/s.

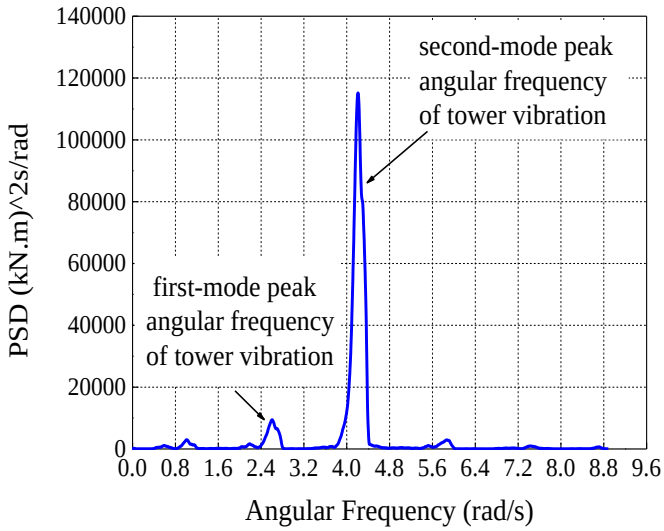

Figure 15. Response spectrum of the wind turbine support tower.

3.4 Mooring system behaviour

Once the entire spar wind turbine system was placed and moored in the model basis, a horizontal stiffness test was conducted to test the restoring capability of the mooring system, both in the surge and sway directions. The directions of surge and sway offset distances and the test results are shown in Figure 16. The model pretension in each mooring line monitored using tension sensors was set to match 2762.375 kN specified for the full scale spar wind turbine configuration.

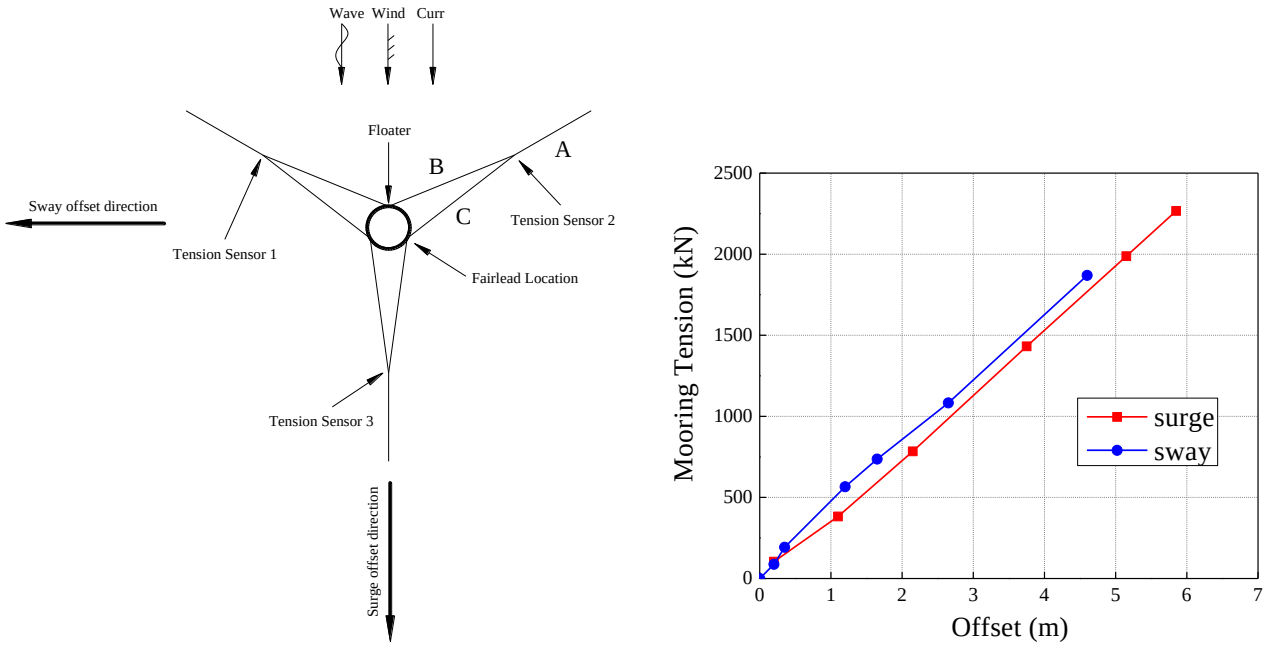

Figure 16. Offset direction illustration and measured horizontal mooring restoring stiffness

As illustrated in Figure 16, the horizontal restoring stiffness in both the longitudinal and transversal directions is relatively large, which means that the floating system will result in a relatively small surge or sway offset when subjected to external loads. This behaviour is consistent with the original intention of the layout design of the delta connection taut mooring system. Additionally, also can be observed is that the surge horizontal stiffness is basically identical with that of the sway.

3.5 spar platform free decay response

Free decay tests were conducted in calm water to identify the natural periods of the integrated floating wind turbine system. The results of the free decay tests for the surge, pitch, heave and yaw are listed in Table 8, as they are the most significant motions for a spar-type floating wind turbine.

Table 8. Results of the free decay tests

Item	Surge	Pitch	Heave	Yaw
Natural period (s)	40.47	33.94	27.54	5.95
Natural angular frequency (rad/s)	0.16	0.19	0.23	1.06
Damping ratio	0.038	0.035	0.028	0.086

3.6 Calibration test of the wave environment

Wave environment was calibrated prior to installation of the model in the basin. Wave elevations were measured at the location where the model will be located. This paper only focus on the two irregular waves utilized in this manuscript and listed in Table 10. These two waves follow a JONSWAP spectrum with significant wave heights of Hs=2.0 and 7.1m. Comparisons of Target and measured spectra for these two waves are shown in Figure 17 and the statistics are compared and listed in Table 9. As can be indicated from Figure 17 and Table 9, it shows a good agreement between the theoretical and basin generated waves.

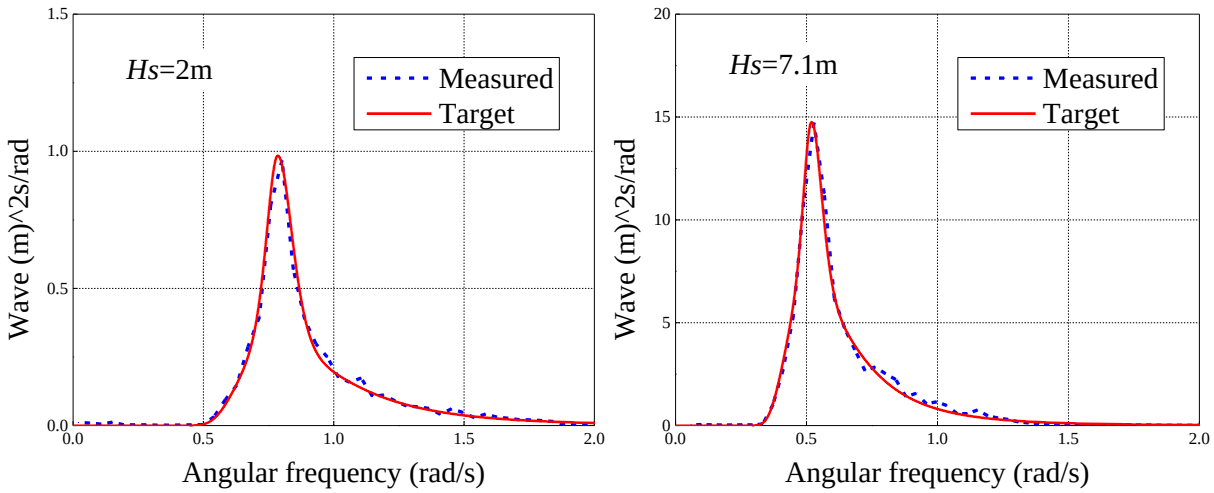

Figure 17. Comparisons of Target and measured spectra for H_s=2.0 and 7.1m JONSWAP irregular waves

Table 9. Statistical comparisons between Target and Measured irregular waves

Item	Units	H_s=2m, T_p=8s, γ=3.3		H_s=7.1m, T_p=12.1s, γ=2.2	
		Measured	Target	Measured	Target
H_s	m	1.99	2.00	7.14	7.10
T_p	s	8.00	8.00	12.10	12.10
Peak angular frequency	rad/s	0.79	0.79	0.52	0.52
Spectrum peak	m^2s/rad	0.96	0.95	14.72	14.56

4. Model test program

To investigate the dynamic response behaviour of a spar-type floating offshore wind turbine, a large scale model basin test program was developed as outlined in Table 10. The test program focused upon three categories including wind only, irregular waves only and the combination of wind and irregular wave conditions. Three prototype wind speeds ranging from 5 m/s to 18 m/s with the corresponding noted rotor speeds are presented. The random wave environment of LC4 was selected to match a one-year return period of the Gulf of Maine (Koo, et al., 2012) and the three parameters are associated with a five-parameter JONSWAP wave amplitude spectrum model. In that model H_s represents the significant wave height, T_p represents the corresponding spectral peak wave period, and γ is a spectral peak parameter where the two peak width parameters are assumed to be the nominally accepted values. Three cases for the combined wind and random seas were investigated. The wave spectrum for the lowest wind speed utilized reduced significant wave height and peak period. The full scale duration of this basin test program lasted about 28 minutes for regular load cases (LC1 to LC3) and lasted 60 minutes for irregular load cases (LC4 to LC7). The initial transients had been removed. And as a uniform sampling frequency, 20 Hz was also selected in this basin test.

Table 10. Case definition and model test program details.

Remark	Load Case	Prototype Wind Speed (m/s)	Rotor Speed (rpm)	H_s (m)	T_p (sec)	γ
Wind Only	LC1	5	7.9	-	-	-
	LC2	11.4	14.4	-	-	-
	LC3	18	10.9	-	-	-

Irregular Waves only	LC4	-	-	7.1	12.1	2.2
Wind with Irregular Waves	LC5	5	7.9	2	8	3.3
	LC6	11.4	14.4	7.1	12.1	2.2
	LC7	18	10.9	7.1	12.1	2.2

5. Characterization of motion and response behaviour

5.1 Effects of rotor rotation on yaw motion

In addition to generating electricity, the wind turbine rotor rotation will excite an extra load (gyroscopic moment) causing an additional contribution to the yaw motion experienced by the floating platform. It is interesting to observe obvious predominant 1P responses in yaw behaviours during model testing procedure, which are closely related to rotor spinning and may be derived from this gyroscopic effect and subsequently dominanted by other corresponding 1P excitations. Similar yaw response characteristics are also found in MARIN's test results (Kimball et al., 2012). The yaw hehaviours are characterized by comparing the wind only cases (LC1, LC2 and LC3) with the combined loading cases (LC5, LC6 and LC7). The wind loads reflected prototype wind speed conditions of 5 m/s, 11.4 m/s and 18 m/s, respectively. The combined loading cases reflected the additional excitation of random waves. The spectral density of the yaw motions based on these six load cases are presented in Figure 18 and summarized in Table 11.

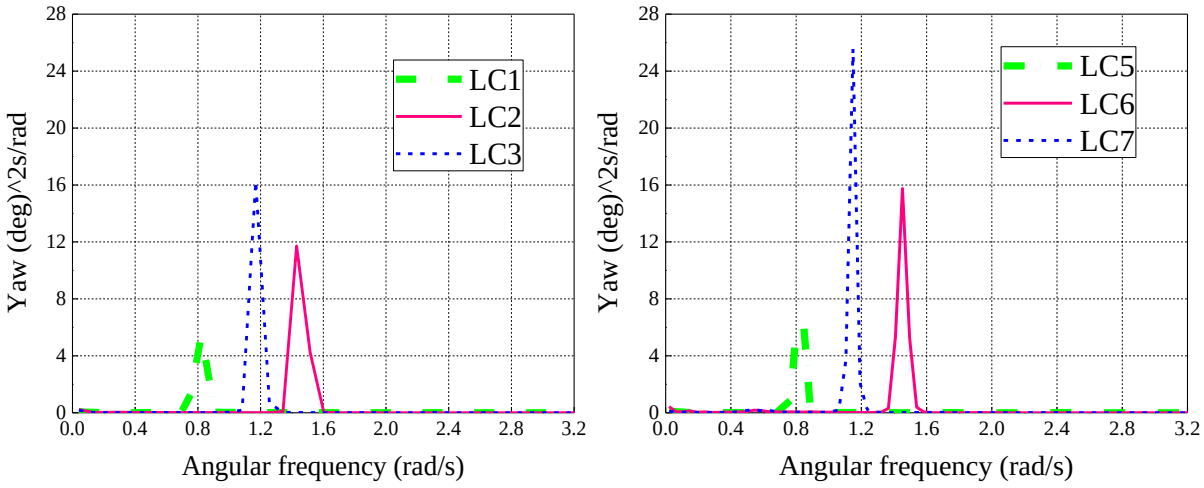

Figure 18. Yaw response spectrum for wind only and wind with wave load cases

Table 11. Comparison between rotation-excited and peak angular frequencies

Item	Unit	LC1	LC2	LC3
Rotation-excited angular frequencies	rad/s	0.827	1.508	1.141
Peak angular frequencies	rad/s	0.822	1.43	1.169

The rotation-excited angular frequencies were estimated from Table 10. Consider the LC1 case where the measured rotation speed of the rotor is 7.9 rpm, meaning that the rotor completes one rotation in 7.595 seconds. The corresponding angular frequency of the rotor rotation is then obtained by dividing 2π by this period, resulting in 0.827 rad/s. It is observed that the angular frequencies of experimentally obtained spectral peaks for the wind only cases are nearly identical with the rotation-excited frequencies, which strongly indicates that the yaw response predominantly oscillates at 1P and is induced by the rotor rotation.

Comparing the spectral data for the wind only and the wind and wave cases it can be observed that the

effect of the irregular waves on the yaw motion is relatively limited. This is because the incoming waves neither excite the resonant responses of yaw at wave angular frequencies nor shift the peak angular frequencies which are induced under wind only conditions. However, the resonant amplitudes of yaw are increased by incoming waves based on a comparison of similar wind speeds. These results demonstrate that the resonance frequency of the yaw motion is dominantly excited by the frequency of the rotor spinning, while the range of yaw fluctuation will be amplified by the incident wave. Furthermore, the rotation-excited yaw motion will affect other responses such as the tower-top bending moment, and these points will be described in detail later.

5.2 Coupled surge, pitch and heave response behaviour

The natural frequencies for the surge, pitch and heave, presented previously in Table 8, are 0.16 rad/s, 0.19 rad/s and 0.23 rad/s, respectively. The combined wind and irregular wave, case LC6, was selected to illustrate the observed coupled response behaviour of surge, pitch and heave. This case involves the highest rotor speed in the test matrix and Figure 19 provides a view overlaying the three spectra. In Figure 19 it is observed that the surge and pitch peaks both occur approximately at a frequency of 0.151 rad/s, which suggests that the resonance response at this frequency is a consequence of the platform being excited by the incident waves near its corresponding natural frequencies. For the same reason, the resonance response of the heave at a frequency of 0.238 rad/s is also controlled by the heave natural frequency. It was observed that there is a long period high amplitude fluctuation in the time history of the surge or pitch motion time series measurements that is a consequence of the unsteadiness of the wind generator that has the same low-frequency behaviour.

The trends observed in each of the spectrum for surge and pitch and even the response induced by the wind generator unsteadiness in the low frequency region are very nearly identical. This indicates that the surge and pitch motions are strongly coupled with one another. The heave motion response has resonances that occur around its natural frequency and at the wave frequency. In the lower frequency range the heave response is significantly different from that of surge and pitch response behaviour. This shows that the heave motion is not subject to any coupling effects and independent from the surge and pitch.

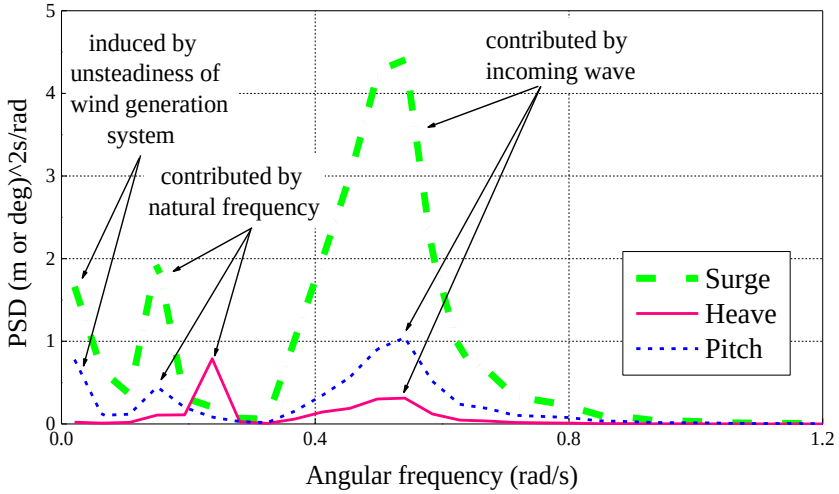

Figure 19. Response spectra for surge, pitch and heave for case LC6

5.3 Suppression effect of aerodynamic loads on motions

In this section the focus is on developing a better understand of the roles of aerodynamic forces and how they influence the motions of a floating wind turbine system. To accomplish this, two cases were selected for comparison, wave only (LC4) and combined wind and wave case LC6, and will be used to study

the surge, pitch and heave response of the floating wind turbine system. The spectrums of each case are overlaid for these motions in Figure 20.

It is observed that the aerodynamic effects neither significantly shift the peak frequencies nor change the peak amplitudes at wave angular frequencies. However, the peak value at lower frequency (near the natural frequency), representing the motion fluctuation in time history, was substantially reduced due to the aerodynamic effect. This is important, as it will benefit the fatigue maintenance of the mooring system.

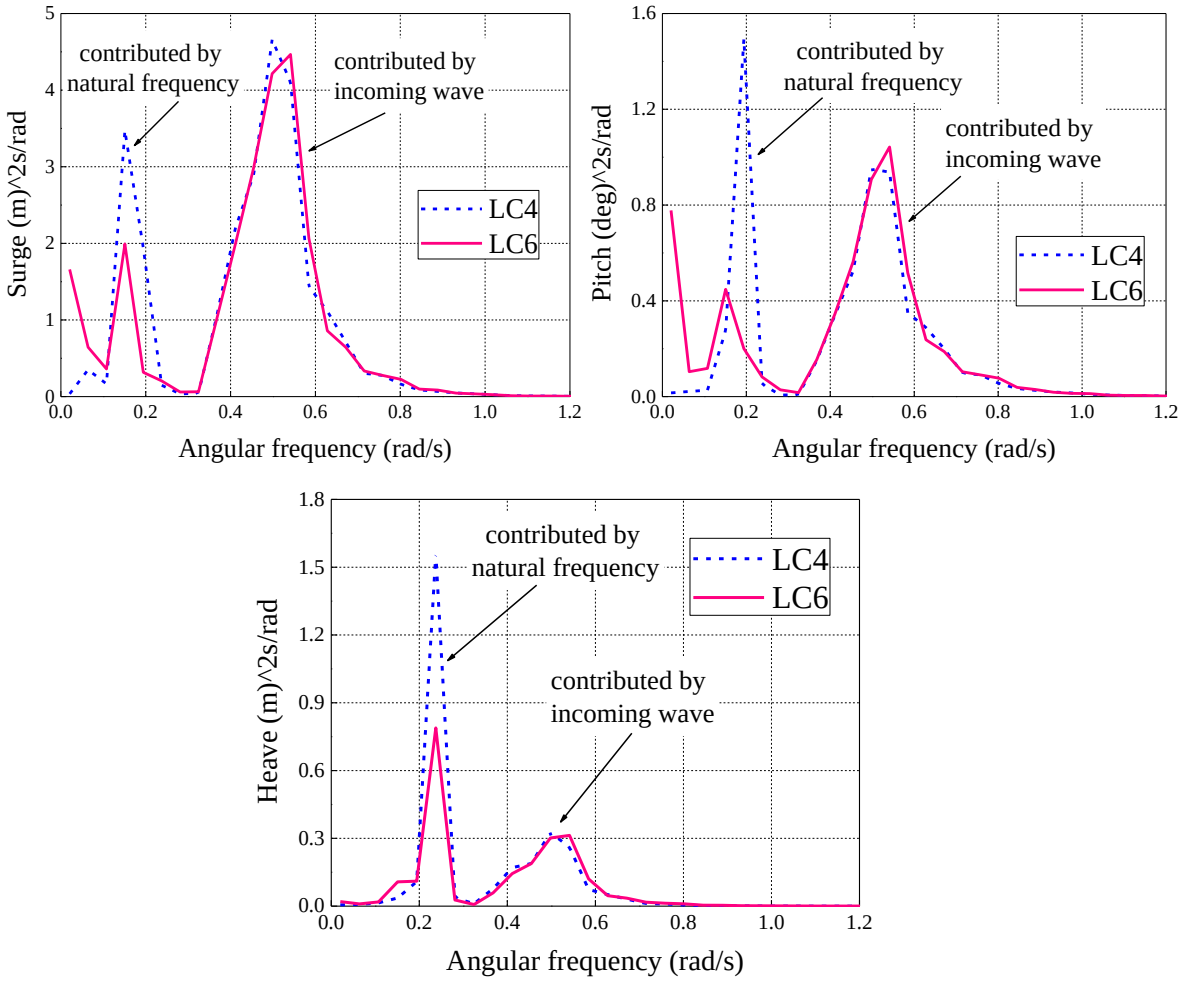

Figure 20. Response spectra for surge, pitch and heave for wave only case LC4 and combined wind and wave case LC6.

5.4 Response behaviour of tower-top bending moment

This section focuses on the tower-top bending moment, and the shear force will be discussed in the next section with the axial rotor thrust. Note that only the Fx1 tower-top shear force, Fx2 axial rotor thrust and My1 tower-top bending moment shown in Figure 8 are analysed in this paper. For simplification, axial rotor thrust means Fx2 force, tower-top shear force and bending moment means Fx1 and My1, respectively.

As noted earlier the rotation-excited yaw motion will affect the tower top bending moment. In order to assess the significance of this contribution wind only cases LC1, LC2 and LC3 were selected for analysis. The spectrum of the tower-top bending moment for these cases are superimposed and presented in Figure 21. Interestingly the peak frequencies of tower-top bending moment spectrum are 0.822 rad/s, 1.43 rad/s and 1.169 rad/s, respectively. These are identical to the peak frequencies for yaw response as listed in Table 11.

This indicates that the fluctuation of the tower-top bending moment is close related to the rotor rotation and rotation-induced yaw under the wind-only conditions. Due to the significant oscillation of the tower-top bending moment observed in Figure 21, attention to this aspect should be considered during the design process.

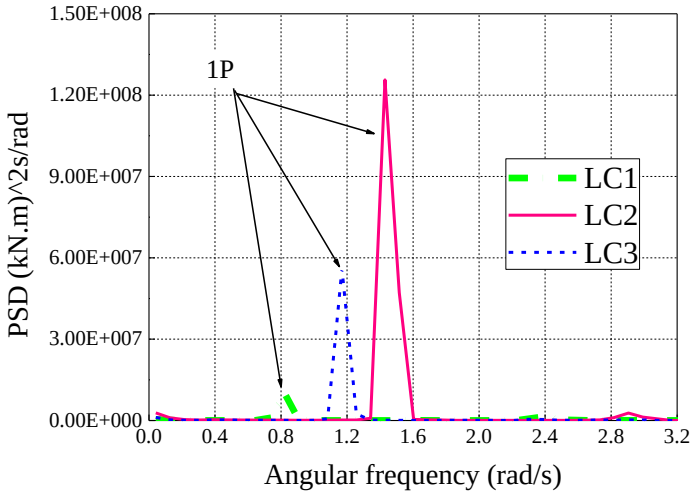

Figure 21. Tower-top bending moment response spectrum for the three wind only cases.

The next aspect to explore is the role of the incoming wave plays on the response behaviour of the tower-top bending moment. Here the wind only case LC2 and the wind-wave case LC6 were selected for further investigation. The spectrum for each case are overlaid and presented in Figure 22.

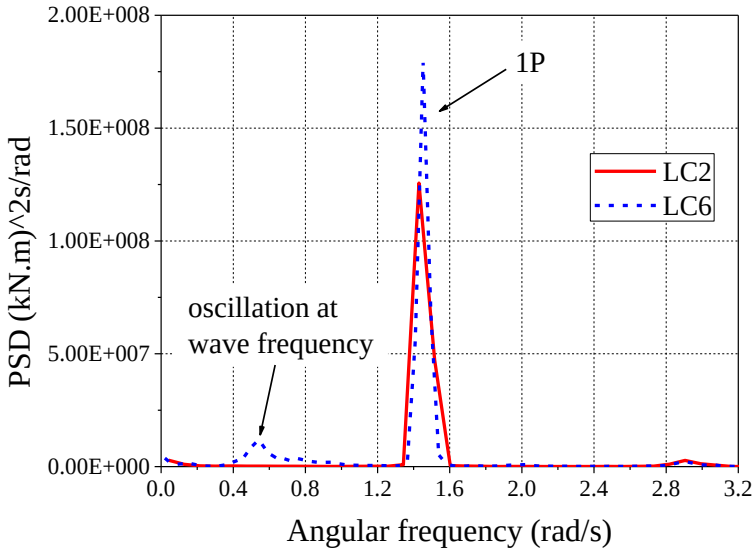

Figure 22. Comparison of tower-top bending moment spectrum for a wind only case LC2, and the combined wind random design sea LC6

Figure 22 clearly demonstrated that the incident wave field significantly amplifies the resonant response component excited at 1P. Also observed is that there exists an additional oscillation component at wave frequency in the response behaviour of the tower-top bending moment when the combined wind-wave

excitation is involved, though this is a much smaller contribution.

5.5 Axial rotor thrust and tower-top shear force

The axial rotor thrust is one of the most important parameters for a floating wind turbine system because it closely relates to the power generation and platform motions, as well as the structural safety of the mooring and integrated floating system. However, due to the manufacturing and installation requirements, the data collected in this model test are not the thrust force applied directly on the hub, but rather contains the inertial force induced by the motor installed in front of the load cell. Even so, the test data can still reflect the major dynamic characteristics of the thrust force generated due to the wind or integrated wind-wave effects. The axial rotor thrust and tower-top shear force are combined together in this section due to their similar dynamic characteristics. To investigate their response characteristics and the relationship between the axial rotor thrust and tower-top shear force, their spectrum for the wind only case LC2 are overlaid and plotted together in Figure 23.

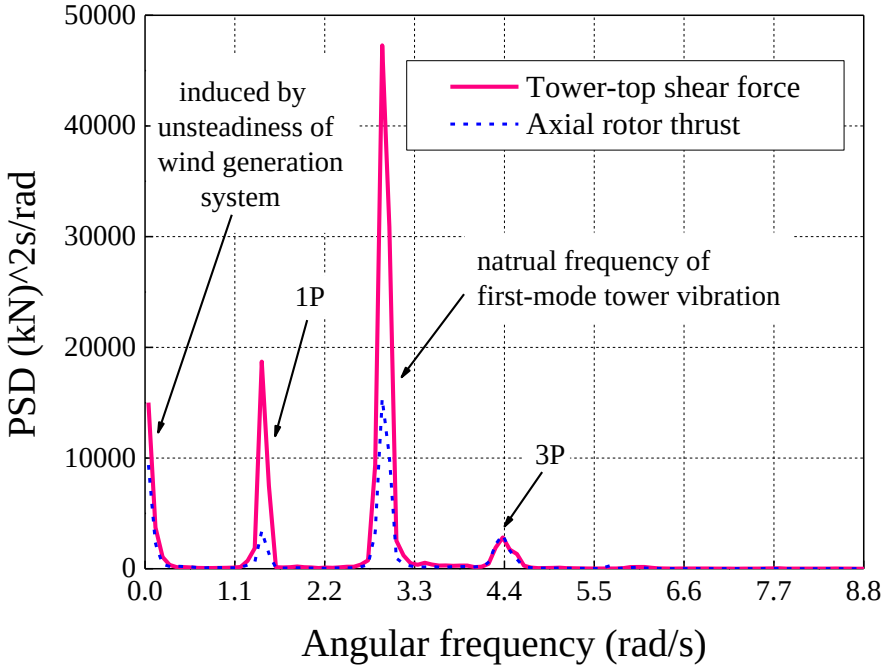

Figure 23. Comparison of the Spectra for tower shear and axial rotor thrust for wind only case LC2.

The PSD of the axial rotor thrust and tower-top shear force shown in Figure 23 are mulit-peaked and each of the various contributions can be identified. The first peak occurs at a frequency of 1.43 rad/s and this corresponds to the rotation-excited yaw motion. The second and largest spectral peak occurs at a frequency of 2.9 rad/s, which is considered to be induced by the first-mode tower vibration. The third peak occurs at 4.38 rad/s, which is close to the 3P frequency (4.29 rad/s). For both the axial rotor thrust and tower-top shear force, the resonance component related to tower's first-mode vibration dominates the other spectral peak contributions. Again the unsteady low-frequency change of wind generation system, which appears as the initial, also exists in the response spectra for axial rotor thrust and tower-top shear force, as shown in Figure 23. Further, the peak amplitude of the axial rotor thrust is smaller than that of the tower-top shear force. This is because the inertial component of the tower-top shear force is due to the entire mass of the nacelle and rotor, whereas for the axial rotor thrust the inertial component is only due to the mass of the rotor and the motor located behind the rotor. This is lighter than the previous mass and results in a smaller inertial force

and subsequently smaller spectrum amplitude. The combined effect of wind and irregular waves on these two types of load can be investigated using the measurements obtained for test case LC6. Figure 24 introduces the spectral results for case LC6, which are plotted with the wind only results of test case LC2.

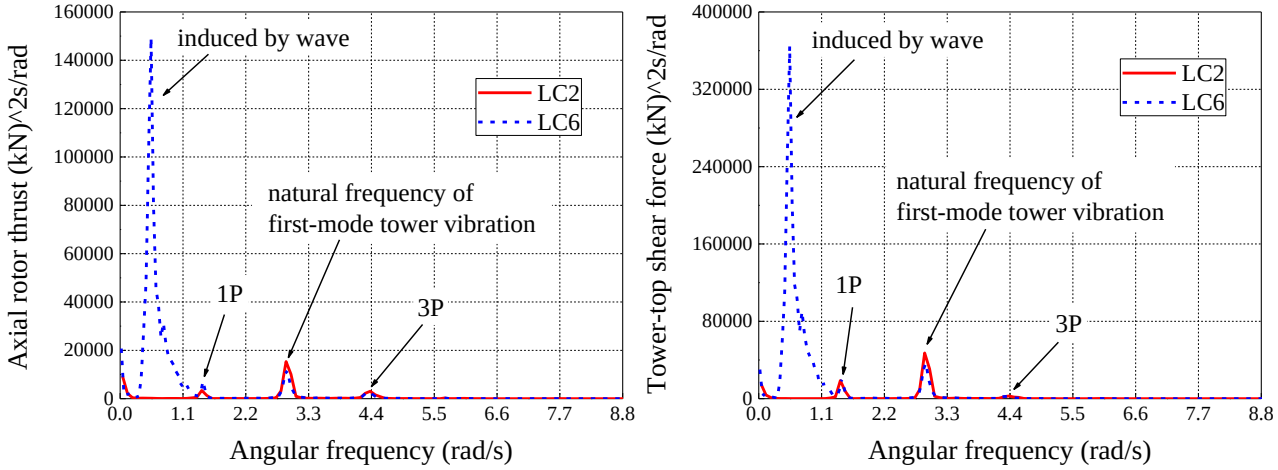

Figure 24. Axial rotor thrust and tower-top shear force for the wind only case LC2 and the wind and irregular wave case LC6.

It is interesting to note the spectral peaks of the axial rotor thrust and tower-top shear force remain nearly identical in amplitude at the same frequencies as the wind only case. There are of course additional response spectral peaks associated with the random seaway that dominate the other spectral peak contributions. Therefore, when experiencing integrated wind-wave loads, the fluctuations of the axial rotor thrust and tower-top shear force are basically due to the incident wave and no longer tower's first-mode vibration any more.

5.6 Mooring system response behaviour

The dynamic characteristics of the mooring system based on wind only, wave only and combined wind and wave loading cases (namely LC2, LC4 and LC6 respectively), are compared and discussed in this section. The mooring system was instrumented with three tension sensors located at the joints of two short mooring lines (B and C lines) to measure the tensions on the mooring lines as illustrated previously in Figure 6. Relative to the tension of mooring line 3 (TOML3), the tension of mooring line 1 (TOML1) and 2 (TOML2) was deemed to be critical based on the direction of the wind and wave loads. It was recognized that because of the symmetry of the mooring system configuration one could have alternatively selected mooring line 2. The spectral response of the TOML2 for the three loading cases is presented in Figure 25.

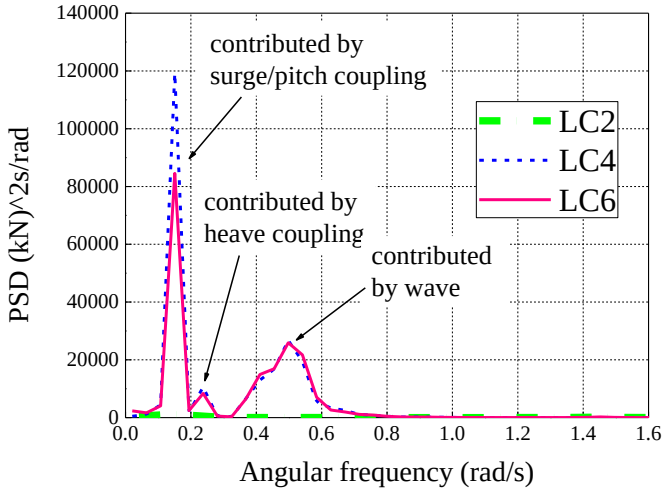

Figure 25. Response spectra of mooring line 2 for wind only case LC2, wave only case LC4 and combined wind and wave case LC6.

As shown in Figure 25, the spectral response behaviour is dominated by the wave-only and the combined wind and wave loading cases. Further, the spectral peak frequencies are 0.151 rad/s, 0.238 rad/s and 0.498 rad/s, respectively. The first two are quite similar with the coupled surge and pitch frequencies and the heave natural frequency for same excitation cases as presented earlier in Figure 19. This demonstrates that the coupled surge and pitch motion and heave motion have an obvious coupling effect on the dynamic response of the mooring system when experiencing wave or wind-wave loading and the surge/pitch coupling influence dominates the other two spectral peak contributions, as shown in Figure 25. The aerodynamic effect of the wind turbine nearly neither shifts the three response peak frequencies nor the peak amplitudes contributed by the heave coupling and the incoming wave. However, the response peaks induced by surge/pitch coupling are seen to be substantially reduced may due to the aforementioned suppression effect of the aerodynamic loads on the surge/pitch response. This oscillation-decreasing characteristic of mooring tensions by aerodynamic loading might benefit the fatigue life of the mooring system.

6. Summary and Conclusions

A model test of a spar-type floating wind turbine system was performed with the purpose of investigating the dynamic characteristics under various load conditions in order to gain insight into the nature of the various load contribution to the complex system response behaviour. Design concepts that involve wind turbines on offshore floating platforms present some challenging scaling issues for model basin tests. In particular it is not possible to simultaneously satisfy Froude scaling for the platform tests and Reynolds scaling for the wind turbine. Froude scaling is used as the basis for the model basin tests, however, issues regarding the aerodynamic modeling mismatch need to be understood when interpreting the test results (Martin et al., 2012). A different approach to previous experiments was taken in allowing the rotor system to freely rotate with the incident wave field. Because of the approach for simulating aerodynamic loading (achieving the correct axial rotor thrust), scaling parameters for the aerodynamic flow are actually not matched well (such as Reynolds number or TSR). This unmatched Reynolds number will result in inaccuracy in some other aerodynamic loads, such as the rotor torque which resulted in an inaccurate model mechanical power. However, that can be accepted because the focus of this basin test is to guarantee the most significant aerodynamic load, the axial rotor thrust, which has a highly close relationship with the 6 DOF motion of the floating system. This strategy is the compromise approach for overcoming the challenging scaling issues, which had also adopted in MARIN' s test (Martin et al., 2012). Besides, Neither pitch control nor measurement of the loads at the interface of the wind turbine support tower was addressed in this study. The

quality of the generated wave field is critical to these types of experiments and in this study it was characterized in terms of spatial velocity and turbulence intensity. Each component and system was carefully calibrated prior to executing the test matrix. The test matrix was designed in a manner to experimentally isolate the effects of wind, waves and the combination of wind and waves.

Based on the analysis of the experimental measurements several interesting response behaviours were observed and are briefly summarized. It was shown that the yaw oscillation response is dominated by the wind turbine rotor rotation and that the fluctuation range of the rotation-induced yaw will be amplified by the incident random waves. Further, the oscillation of tower-top bending moment is dominated by the 1P resonant response when only wind excitation of the wind turbine is involved. The presence of waves will amplify the range of this oscillation component and excites a spectral peak at the wave frequency which quite small. As expected for spar platforms excited by design seas the surge and pitch motions are strongly coupled, and the heave motion is independent from surge and pitch. The spectral response of the mooring system, also reflects the surge and pitch coupling. The effect of the aerodynamic excitation on the surge, pitch and heave response behaviour basically remain at the same frequencies but the peak amplitudes are somewhat reduced. This is also reflected in the mooring line tension measurements and this could be beneficial in extending the fatigue life of the mooring system. It was observed that the axial rotor thrust and tower-top shear force have similar dynamic characteristics. When only the wind excitation of the wind turbine is present, they both oscillate at 1P, tower first-mode natural frequency and 3P. And they are both dominated by the tower's first mode of vibration. However, when the combined wind wave excitation is involved, the responses of the axial rotor thrust and tower-top shear force are dominated by the incident wave field.

The model study was carefully designed and executed to provide both new insights into the complex system response of spar-type wind turbine and to provide data complementing earlier research studies on this topic. Further, this study focused only on the analysis of the experimental measurement data and numerical simulation comparisons are the subject of ongoing research studies. In the future works, researcheres can establish the FOWT model in their simulation tools and validate their codes by ultilizing results presented in this manuscript. Additionally, though interesting dynamic response characteristics of FOWT are presented and corresponding analysis are conduced, more deeply investigations can be further implemented. Based on this test, specific tests that aimed to investigate the inherent cause of some response characteristic phenomenon can be conducted in the future. Also, a numerical model can be built in the simulation tools whose accuracy can be validated by the results of this work. Then, from simulation, some special data can be obtained (e.g. loads in the blade or deformations in the blade). By analyzing these variables behaviors, the inherent reasons for some particular phenomenons are able to be more clearly revealed. And correeponding predicitions can also be further employed.

Acknowledgements

The first two authors gratefully acknowledge the financial support for this research from the Natural Science Fund of China (Grant No. 51239007) and State Key Lab of Ocean Engineering at Shanghai Jiao Tong University for the model test program support. The third author gratefully acknowledges the financial support of the Wofford Cain'13 Senior Endowed Chair in Offshore Technology, the Texas A&M Engineering Experiment Station and the continued collaborative spirit of the faculty and their students in the Department of Naval Architecture, Ocean and Civil Engineering at Shanghai Jiao Tong University.

References

[1] Sclavounos P, Tracy C, Lee S. Floating Offshore Wind Turbines: Responses in a Sea state Pareto

Optimal Designs and Economic Assessment. OMAE2008-57056, Estoril, Portugal; 2008.

[2] Namik H, Stol K. Individual Blade Pitch Contorl of Floating Offshore Wind Turbines. Wind Energy 2010;13(1):74-85.

[3] Wang L, Sweetman B. Multibody dynamics of floating wind turbines with large-amplitude motion. Applied Ocean Research 2013; 43: 1-10.

[4] Jeon M, Lee S, Lee S. Unsteady Aerodynamics of Offshore Floating Wind Turbine in Platform Pitching Motion Using Vortex Lattice Method. Renewable Energy 2014; 65:207-212.

[5] Salehyar S, Zhu Q. Aerodynamic dissipation effects on the rotating blades of floating wind turbines. Renewable Energy 2015; 78:119-127.

[6] Nejad A R, Bachynski E E, Kvittem M I, Luan C Y, Gao Z, Moan T. Stochastic dynamic load effect and fatigue damage analysis of drivetrains in land-based and TLP, spar and semi-submersible floating wind turbines. Marine Structures 2015;42:137-153.

[7] Jonkman J, Butterfield S, Musial W, Scott G. Definition of a 5-MW Reference Wind Turbine for Offshore System Development. Technical Report NREL/TP-500-38060. National Renewable Energy Laboratory (NREL); 2009.

[8] Jonkman J. Definition of the Floating System for Phase IV of OC3. Technical Report NREL/TP-500-47535. National Renewable Energy Laboratory (NREL); 2010.

[9] Jonkman J, Robertson A, Popko W, Vorpahl F, Zuga A, Kohlmeier M, Larsen T J, Yde A, Saetertro K, Okstad K M, Nichols J, Nygaard T A, Gao Z, Manolas D, Kim K, Yu Q, Shi W, Park H, Rojas A V, Dubois J, Kaufer D, Thomassen P, de Ruiter M J, Peeringa J M, Zhiwen H, Waaden H V. Offshore Code Comparison Collaboration Continuation (OC4), Phase I – Results of Coupled Simulations of an Offshore Wind Turbine with Jacket Support Structure. Technical Report NREL/CP-5000-54124. National Renewable Energy Laboratory (NREL); 2012.

[10] Robertson A, Jonkman J, Musial W. Offshore Code Comparison Collaboration, Continuation: Phase II Results of a Floating Semisubmersible Wind System. Technical Report NREL/CP-5000-60600. National Renewable Energy Laboratory (NREL); 2013.

[11] Karimirad M. Stochastic Dynamic Response Analysis of Spar-Type Wind Turbines with Catenary or Taut Mooring Systems. Ph.D. Thesis. Norwegian University of Science and Technology; 2011.

[12] Kvittema M I, Bachynski E E, Moan T. Effects of Hydrodynamic Modeling in Fully Coupled Simulations of a Semisubmersible-Submersible Wind Turbine. Energy Procedia 2012; 24: 351-362.

[13] Quallen S, Xing T, Carrica P, Li Y W, Xu J. CFD Simulation of a Floating Offshore Wind Turbine System Using a Quasi-Static Crowfoot Mooring-Line Model. In: Proceedings of the Twenty-third (2013) International Offshore and Polar Engineering, Anchorage, Alaska, USA; ISOPE 2013.

[14] Bae Y H, Kim M H, Shin Y S. Rotor-floater-mooring Coupled Analysis of Mini-TLP-Type Offshore Floating Wind Turbines. In: Proceedings of the ASME 2010, 29th International Conference on Ocean, Offshore and Arctic Engineering, Shanghai, China; 2010. Paper no. OMAE2010-20555

[15] Gueydon S, Xu W. Floating Wind Turbine Motion Assessment. Oceans 2011 Conference, Kona, Hawaii, USA; 2011.

[16] Nielsen F G, Hanson T D, Skaare B. Integrated Dynamic Analysis of Offshore floating Wind Turbines. Hydro Oil & Energy, Hamburg, Germany; 2006.

[17] Cermelli C, Aubault A, Roddier D, McCoy T. Qualification of a Semi-Submersible Floating Foundation for Multi-Megawatt Wind Turbines. Offshore Technology Conference, Houston, USA; 2010.

[18] Shin H. Model Test of the OC3-Hywind Floating Offshore Wind Turbine. In: Proceedings of the Twenty-first (2011) International Offshore and Polar Engineering Conference, Maui, HI, USA; ISOPE 2011; page: 361-367.

[19] WindSea website. http://www.windsea.no/, accessed January 2012.

[20] Martin H R, Kimball R W, Viselli A M, Goupee A J. Methodology for Wind/Wave Basin Testing of

Offshore floating Wind Turbines. In: Proceedings of the ASME 2012, 31st International Conference on Ocean, Offshore and Arctic Engineering, Rio de Janeiro, Brazil; 2012. Paper no. OMAE2012-83627.

[21] Koo B, Goupee A J, Lambrakos K, Kimball R W. Model Tests for a Floating Wind Turbine on Three Different Floaters. In: Proceedings of the ASME 2012, 31st International Conference on Ocean, Offshore and Arctic Engineering, Rio de Janeiro, Brazil; 2012. Paper no. OMAE2012-83642.

[22] Goupee A J, Koo B, Kimball R W, Lambrakos K F, Dagher H J. Experimental Comparison of Three Floating Wind Turbine Concepts. In: Proceedings of the ASME 2012, 31st International Conference on Ocean, Offshore and Arctic Engineering, Rio de Janeiro, Brazil; 2012. Paper no. OMAE2012-83645.

[23] Huijs F, de Ridder E J, Savenije F. Comparison of Model Tests and Coupled Simulations for a Semi-submersible Floating Wind Turbine. In: Proceedings of the ASME 2014, 33rd International Conference on Ocean, Offshore and Arctic Engineering, San Francisco, California, USA; 2014. Paper no. OMAE2014-23217.

[24] Wan L, Gao Z, Moan T. Model Test of the STC Concept in Survival Modes. In: Proceedings of the ASME 2014, 33rd International Conference on Ocean, Offshore and Arctic Engineering, San Francisco, California, USA; 2014. Paper no. OMAE2014-23213.

[25] Gueydon S, Weller S. Study of a Floating Foundation for Wind Turbines. In: Proceedings of the ASME 2012, 31st International Conference on Ocean, Offshore and Arctic Engineering, Rio de Janeiro, Brazil; 2012. Paper no. OMAE2012-83389.

[26] Coulling A, Goupee A, Robertson A, Jonkman J. Importance of Second-Order Difference-Frequency Wave-diffraction Forces in the Validation of a Fast Semi-submersible Floating Wind Turbine Model. In: Proceedings of the ASME 2013, 32nd International Conference on Ocean, Offshore and Arctic Engineering, Nantes, France; 2013. Paper no. OMAE2013-10308.

[27] Koo B, Goupee A, Lambrakos K, Lim H. Model Test Data Correlations with Fully Coupled Hull/Mooring Analysis for a Floating Wind Turbine on a Semi-Submersible Platform. In: Proceedings of the ASME 2014, 33rd International Conference on Ocean, Offshore and Arctic Engineering, San Francisco, California, USA; 2014. Paper no. OMAE2014-24254.

[28] Allen C, Goupee A, Dagher H, Viselli A. Validation of Global Performance Numerical Design Tools Used for Design of Floating Offshore Wind Turbines. In: Proceedings of the ASME 2015, 34th International Conference on Ocean, Offshore and Arctic Engineering, St. John's, NL, Canada; 2015. Paper no. OMAE2015-41437.

[29] Huijs F. The Influence of the Mooring System on the Motions and Stability of a Semi-submersible Floating Wind Turbine. In: Proceedings of the ASME 2015, 34th International Conference on Ocean, Offshore and Arctic Engineering, St. John's, NL, Canada; 2015. Paper no. OMAE2015-41947.

[30] Robertson A, Jonkman J, Goupee A, Coulling A, Prowell I, Browning J, Masciola M, Molta P. Summary of Conclusions and Recommendations Drawn from the DeepCwind Scaled Floating Offshore Wind System Test Campaign. In: Proceedings of the ASME 2013, 32nd International Conference on Ocean, Offshore and Arctic Engineering, Nantes, France; 2013. Paper no. OMAE2013-10817.

[31] Martin H R. Development of a Scale Model Wind Turbine for Testing of Offshore Floating Wind Turbine Systems. M.S. Thesis, The University of Maine, United States of America; 2011.

[32] Coulling A J, Goupee A J, Robertson A N, Jonkman J M, Dagher H J. Validation of a FAST semi-submersible floating wind turbine numerical model with DeepCwind test data. Journal or Renewable and Sustainable Energy 5, 023116; 2013.

[33] Duan F, Hu Z Q, Wang J. Model Tests of a Spar-type Floating Wind Turbine under Wind/Wave Loads. In: Proceedings of the ASME 2015, 34th International Conference on Ocean, Offshore and Arctic Engineering, St. John's, NL, Canada; 2015. Paper no. OMAE2015-41391.

[34] Fowler M J, Kimball R W, Thomas III D A, Goupee A J. Design and Testing of Scale Model Wind Turbines for Use in Wind/Wave Basin Model Tests of Floating offshore Wind Turbines. In: Proceedings of the ASME 2013, 32nd International Conference on Ocean, Offshore and Arctic Engineering, Nantes, France; 2013. Paper no. OMAE2013-10122.

[35] Kimball R W, Goupee A J, Coulling A J, Dahger H J. Model Test Comparisons of TLP, Spar-buoy and Semi-submersible Floating Offshore Wind Turbine Systems. SNAME conference; 2012. Paper no. SNAME-016-2012.